SHEAR-WAVE ANISOTROPY BY ALIGNED CRACKED INCLUSIONS: FREQUENCY AND ATTENUATION PROPERTIES

J. J. S. de Figueiredo, R. R. Stewart, J. Schleicher, N. Dyaur, B. Omoboya, R. Wiley, and A. William

email: *jadsomjose@gmail.com and js@ime.unicamp.br*
keywords: *Shear-wave anisotropy, frequency analysis, crack media attenuation*

ABSTRACT

Anisotropic cracked media have been widely investigated in many theoretical and experimental studies. In this work, we have performed ultrasonic surveys to investigate the influence of source frequency on elastic parameters (the Thomsen parameter γ and shear-wave attenuation) of fractured anisotropic media. Under controlled conditions, we prepared anisotropic models containing penny-shaped rubber inclusions in a solid epoxy resin matrix with crack density that ranges from 0 to 6.2 %. Two of the three cracked models have 10 layers and the last one has 17 layers. The number of uniform rubber inclusions per layer was from 0 up to 100. S-wave splitting measurements have shown that scattering effects are more prominent in models where the crack aperture to seismic wavelength ratio ranges from 1.6 to 13.3 than in other models where the ratio varied from 2.3 to 23. The model with large cracks gave a magnitude of attenuation 3 times higher compared with another model that had small inclusions. These results indicate that elastic scattering, intrinsic and scattering attenuation (Q_{in}^{-1} and Q_s^{-1} respectively), and velocity dispersion directly interfere in shear wave splitting, which in turn is a function of crack size and source frequency.

INTRODUCTION

Wave propagation in anisotropic cracked and fractured media has motived many studies in seismic exploration of hydrocarbons reservoirs. Because of the geologic complexities exhibited by anisotropic media, reliable conclusions about elastic properties are usually difficult to achieve with accuracy from field data. On the other hand, laboratory measurements have been shown to be a useful tool for modeling conditions present in the field, helping to reduce uncertainty about elastic parameters in numerical methods.

It is well known that numerical simulation of cracked media is computationally and mathematically expensive and intense (Hudson, 1981; Crampin, 1981; Hudson et al., 2001). Furthermore, when scattering effects are taken into account, these costs become even more significant (Willis, 1964; Mal, 1970; Yang and Turner, 2003, 2005). Nonetheless, some difficulties of anisotropic modeling can be overcome using experimental scaled physical modeling.

Assad et al. (1992, 1996), Wei (2004) and Wei et al. (2007) established an experimental relationship between crack density and shear velocity based on theoretical predictions by Hudson (1981). Melia and Carison (1984) carried out a series of experiments in anisotropic samples to investigate P-wave dispersion in anisotropic layered media as a function of the concentration of different layered materials as well as the thickness of the layers. Based on the same approach, Marion et al. (1994) and Rio et al. (1996) showed the influence of short and long wavelengths in stratified media as well as wave velocity dispersion and multiple scattering.

Other sets of experimental observations performed by Rathore et al. (1995) and Peacock et al. (1994) demonstrated the feasibility of the ultrasonic approach to investigate artificially cracked porous media.

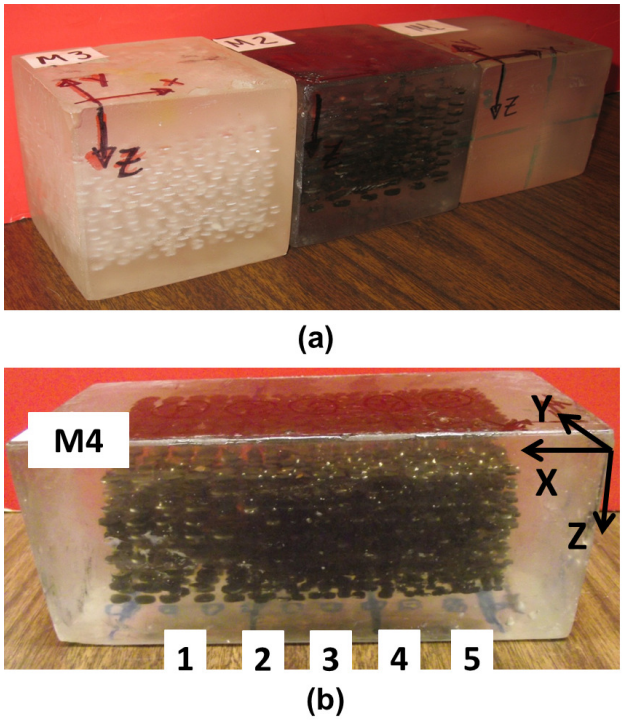

Figure 1: (a) From right to left: Reference model M1 (uncracked) and cracked models M2, M3; (b) model M4. Also shown are the orientations of the coordinate systems. All wave measurements were made in the Y direction.

Using experimental data obtained by Rathore et al. (1995), the theoretical predictions of Thomsen (1995) for aligned cracks in porous rock received a strong support. More recently, experiments by Tillotson et al. (2011) have suggested the possible use of shear wave data to discriminate fluids on the basis of viscosity variations.

In anisotropic cracked media, the frequency response is influenced by the size of the heterogeneities. However, quantification of this influence is still desirable. To better understand the influence of frequency on cracked materials, we conducted a series of experiments aimed at extending previous approaches by using a shear-wave source with different frequencies: low frequency (LF $= 90$ kHz), intermediate frequency (IF $= 431$ kHz) and high frequency (HF $= 840$ kHz). We carried out experiments on a reference model without inclusions and three other models with different inclusion sizes, thereby simulating different crack densities. In this arrangement, shear-wave splitting was observed with different magnitudes as a function of frequency. Our results show that effects associated with intrinsic (Q^{-1}) and scattering (Q_s^{-1}) attenuation (Gorich and Muller, 1987; Tselentis, 1998) interfere directly with shear wave splitting, which in turn is related to crack density. Furthermore, we observed that the anisotropic parameter γ (Thomsen, 1986) varies with frequency and crack size. For these purposes, we quantified attenuation using the frequency shift method (Quan and Harris, 1997).

EXPERIMENTAL PROCEDURE

The construction of the cracked samples as well as the ultrasonic measurements were carried out at the Allied Geophysical Laboratories (AGL) at the University of Houston.

Model preparation

Under controlled conditions, we constructed three cracked models (M2, M3, and M4) with different crack densities and one uncracked model (M1) for reference. Pictures of all models are shown in Figure 1. Model M4 has five different points that can be analyzed. The same distance between layers (0.5 cm for M2 and M4 and 0.25 cm for M3) was ensured by using the same volume of epoxy resin poured for each layer.

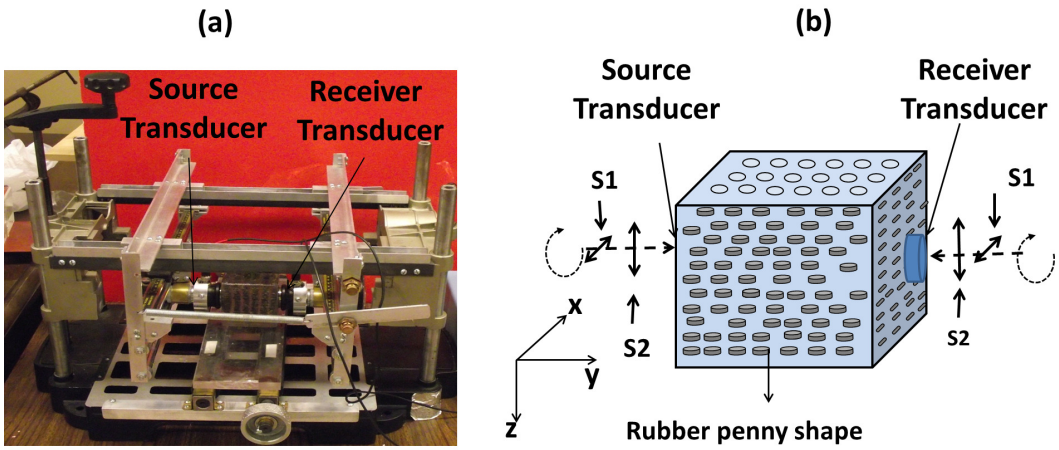

Figure 2: (a) Device developed for S-wave polarization rotation. (b) Sketch of experiment used for seismogram records.

Each layer with inclusions was added to the model and air was extracted using a vacuum pump to avoid inhomogeneities in the epoxy resin. The crack density ε in the cracked models was determined by

$$\varepsilon = \frac{N\pi r^2 h}{V}\,, \tag{1}$$

where N is total number of inclusions, r is their radius, h is inclusions' thickness (aperture of cracks), and, finally, V is the total model volume. Equation (1) is a modification of the relation of Hudson (1981) for crack density estimation.

The ratio of compressional wave velocity between solid epoxy and neoprene was around 1.5 and for solid epoxy and silicone rubber was about 2.25. The S-wave velocity in rubber was difficult to determine because of the low shear modulus of this material. The parameters of the included rubber cracks in each model are displayed in Table 1.

Model	Crack density (%)	Measuring length (cm)	Number of layers	Diameter (cm)	Aperture (cm)	Cracks per layer	Aspect ratio
M1	Isotropic	7.31 ± 0.02	0	-	-	0	0
M2	4.5	7.29 ± 0.02	10	0.7	0.091	36	0.13
M3	3.8	7.32 ± 0.02	17	0.4	0.051	90	0.12
M4-1	6.0	7.64 ± 0.02	10	0.7	0.091	30	0.13
M4-3	5.2	7.74 ± 0.02	10	0.44	0.091	80	0.20
M4-5	4.2	7.74 ± 0.02	10	0.32	0.091	100	0.28

Table 1: Physical parameters of models M1, M2, M3 and M4

Ultrasonic measurements

Over these models, we carried out ultrasonic measurements using the Ultrasonic Research System at AGL with the pulse transmission technique. The sampling rate per channel for all experiments was 10 MHz. Figure 2a shows a device developed for recording S-wave seismograms. The source and receiver transducers were arranged on opposing sides of the model, separated by measuring length (see Table 1). The initial shear-wave polarization was parallel to the cracks. Changes in polarization were achieved by rotating both transducers by 10 degrees at a time until polarization was again parallel (i.e., 0 to 180 degrees) to the XZ plane (see Figure 2b). In total, 19 traces were recorded in each seismic section with 20fold stack to eliminate ambient noise. The polarizations of 0 and 180 degrees correspond to the fast S-wave (S1) and 90 degrees corresponds to the slow S-wave (S2).

Figure 3a and b shows the S-wave signature sources and Fourier amplitude spectra of the three sources used to obtain the data shown in this paper. We performed a Gaussian non-linear fit in each frequency

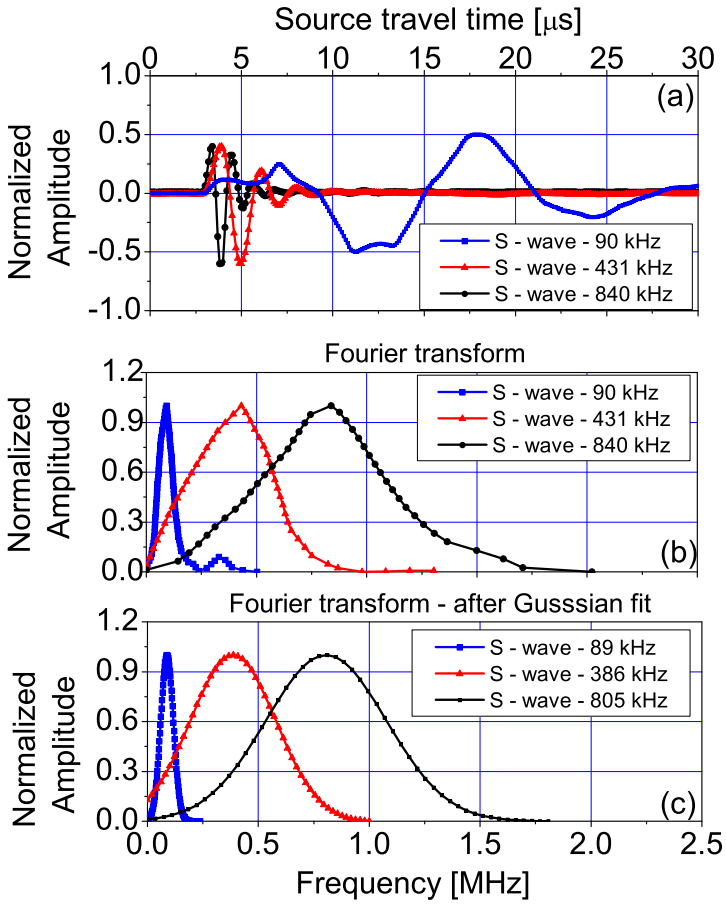

Figure 3: S-wave source signature of LF $=$ 90 kHz, IF $=$ 430 kHz and HF $=$ 840 kHz. (b) Fourier transform of each signature trace. (c) Fourier transform after Gaussian nonlinear fit. Here the dominant frequencies have become 89 kHz, 386 kHz and 805 kHz.

distribution, which is depicted in Figure 3c. We used this fit to obtain the centroid frequency as well the variance of frequency content. This information is required for the attenuation estimation using the frequency shift method (Quan and Harris, 1997). The delay time in all S-wave transducers was 2.7 μs (see Figure 3a). For the velocity calculation, the delay time was subtracted from the observed arrival time. The accuracy of time picking was ± 0.1 μs, which allows to determine the wave velocities with an accuracy of $\pm 0.3\%$.

EXPERIMENTAL RESULTS

In this section, we discuss our experimental results for S-wave splitting in three cracked models and one uncracked model, including a frequency-domain attenuation analysis in the three different frequency ranges (LF, MF and HF).

Shear wave seismograms

We observed shear-wave splitting for all frequencies in models M2 and M3. The magnitude of this birefringence also appears to depend on the frequency of the source. Figures 4, 5 and 6 show the seismograms recorded in models M1, M2 and M3 for low, intermediate and high frequency sources, respectively. As expected, the isotropic model (M1) shows uniform first arrivals for all polarizations and all recording frequencies, not separating fast (S1, 0^0 and 180^0) and slow (S2, 90^0) S-waves.

In model M2, the splitting observed between the fast and slow shear waves was 6.9 μs for LF data (Figure 4) and 1.7 μs for IF data (Figure 5). In model M3 (with a higher density of smaller cracks), the

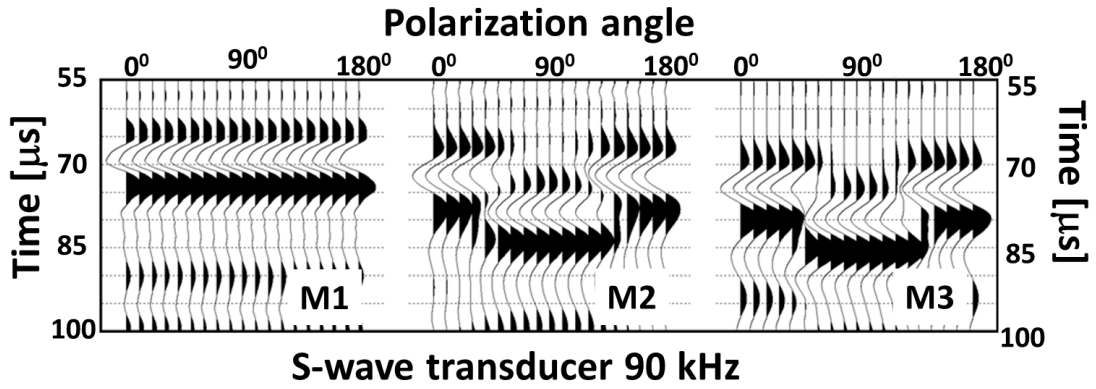

Figure 4: S-wave seismograms as a function of change in polarization from 0^0 to 180^0 for models M1 (isotropic), M2 and M3 in the LF range.

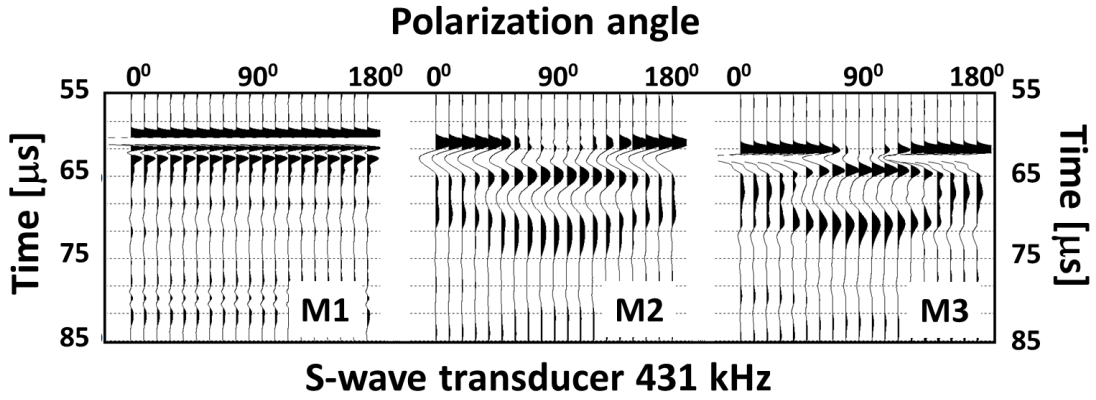

Figure 5: S-wave seismograms as a function of change in polarization from 0^0 to 180^0 for models M1 (isotropic), M2 and M3 in the IF range.

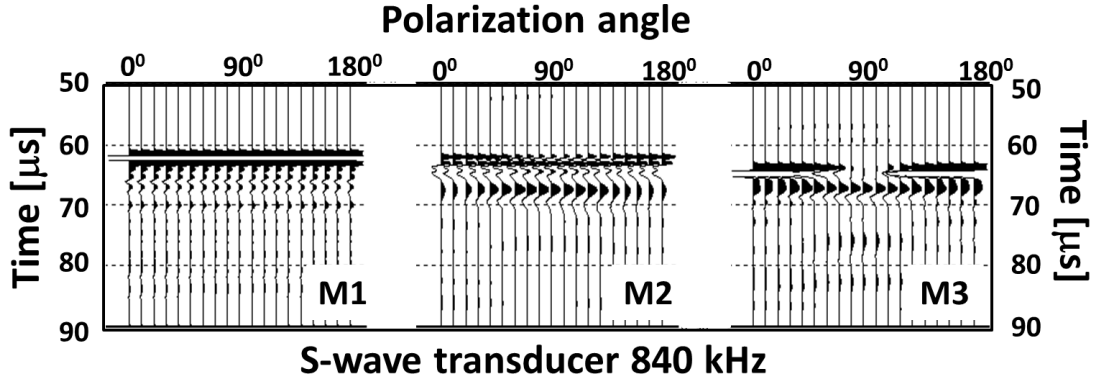

Figure 6: S-wave seismograms as a function of change in polarization from 0^0 to 180^0 for models M1 (isotropic), M2 and M3 in the HF range.

values of splitting were smaller. We found 3.9 μs and 1.5 μs for LF and IF data, respectively (see Figures 4 and 5). In the case of the high frequency measurement, model M2 (see Figure 6) shows inconsistent fast and slow shear wave arrivals, which probably can be attributed to the pulse wavelength being of the same order as the size of the crack aperture. We will elaborate on this assumption in a later section. Similarly, due to the small ratio between wavelength and crack aperture, the model M3 for HF source presents a splitting of 0.8 μs.

Frequency analysis

Figure 7 shows the Fourier spectra of the seismograms and their respective Gaussian non-linear fit spectra for model M1. We observe that in this isotropic epoxy resin, the HF waves are the most strongly attenuated ones. Their dominant frequency is shifted from 840 kHz (source frequency) to 519 kHz (frequency response), while the shift for IF is from 431 kHz to 317 kHz and the one for LF is 090 kHz to 88 kHz.

The corresponding results for models M2 are depicted in Figures 8. In this model, the ratio of wavelength to crack aperture ranges from 1.3 to 13.3 and hence effects associated with scattering or diffraction as well as effective media are expected to be seen at the same time (Matsushima et al., 2011; Gibson et al., 2000; Marion et al., 1994). In the HF response (see Figure 8c), we observe two independent peaks for both the S1 and S2 waves. The reason is that the high-frequency contributions of the wavefield travel unaffected in the homogeneous medium between the cracks, giving rise to an unperturbed first arrival of the observed wavefield (see Figure 6). Low-frequency contributions propagate as if in an effective medium, almost unperturbed from the individual cracks, because the crack size is much smaller than the wavelength. On the other hand, intermediate frequency with wavelengths of the order of the size of the scatterers suffer from the strongest attenuation and scattering. Thus, these effects result in two peaks at either side of the original source spectrum. Note that Figures 8a and b do not exhibit the second peak, indicating that the high frequencies that suffer very little attenuation are not present in these wavefields. This is evidenced in Table 2, which presents the ratio between crack aperture and seismic wavelength for S1 and S2 waves in models M2 and M3 in the LF, IF, and HF range.

	(90 kHz)		(431 kHz)		(840 kHz)	
Model	$\frac{\lambda_{S1}}{aper}$	$\frac{\lambda_{S2}}{aper}$	$\frac{\lambda_{S1}}{aper}$	$\frac{\lambda_{S2}}{aper}$	$\frac{\lambda_{S1}}{aper}$	$\frac{\lambda_{S2}}{aper}$
M2	14.89	13.33	3.16	2.88	1.64	1.60
M3	26.31	24.68	5.54	5.231	2.85	2.72

Table 2: The crack aperture to seismic wavelength ratio for polarizations S1 and S2.

Two other observations are worth noting in Figure 8c. (1) There is a strong shift of dominant frequency as compared to the source. This shift is stronger for the S1 polarization (from 840 khz to 172 khz) than for S2 (from 840 khz to from 219 khz). (2) The second peak is much more pronounced for the S2 polarization than for S1.

The strong frequency shift for both polarizations may be explained by the fact that the inclusion lengths are greater than the source's dominant wavelength, which increases the scattering-related attenuation (see Table 2). The fact that the second peak is much stronger for the S1 than for the S2 polarization indicates that scattering is dominant when the polarization is parallel to the crack, but that attenuation becomes more important when the polarization is perpendicular to the cracks. Strong shifts of the dominant frequencies of the S1 and S2-wave polarizations also can be noted for IF (see Figure 8b).

For a better understanding of the two separate peaks, we applied a band-pass filter of 10-50-350-400 kHz to the HF data of model M2. The result is depicted in Figure 9b. The part of the seismogram associated with acoustic scattering or diffraction due to HF is shown in Figure 9c. Note that after filtering, shear-wave splitting with a magnitude of 1.4 μs becomes visible (Figure 9b), which could not be observed before. This corroborates our interpretation that the low-frequency part of the wavefield behaves as if traveling in an effective anisotropic medium. On the other hand, the seismic section associated with the peaks at 750 kHz and 820 kHz can be observed in the Figure 9c. No shear-wave splitting is visible, indicating that the high-frequency part of the wavefield behaves as if traveling in an isotropic medium.

In model M3, none of the frequency ranges produces a second peak (see Figure 10), because the cracks are too small and too densely distributed to allow for unperturbed wave propagation in the homogeneous background model. However, as can be noted, in this model the shift in frequency associated with the perpendicular polarization (S2) is more prominent than for S1. As mentioned before, the pulse wavelength to crack aperture ratio for M3 ranges from 1.2 to 2.3, and the wavelengths are not much smaller than the crack size. This explains why there is less unscattered wave propagation and less unperturbed energy as compared to model M2.

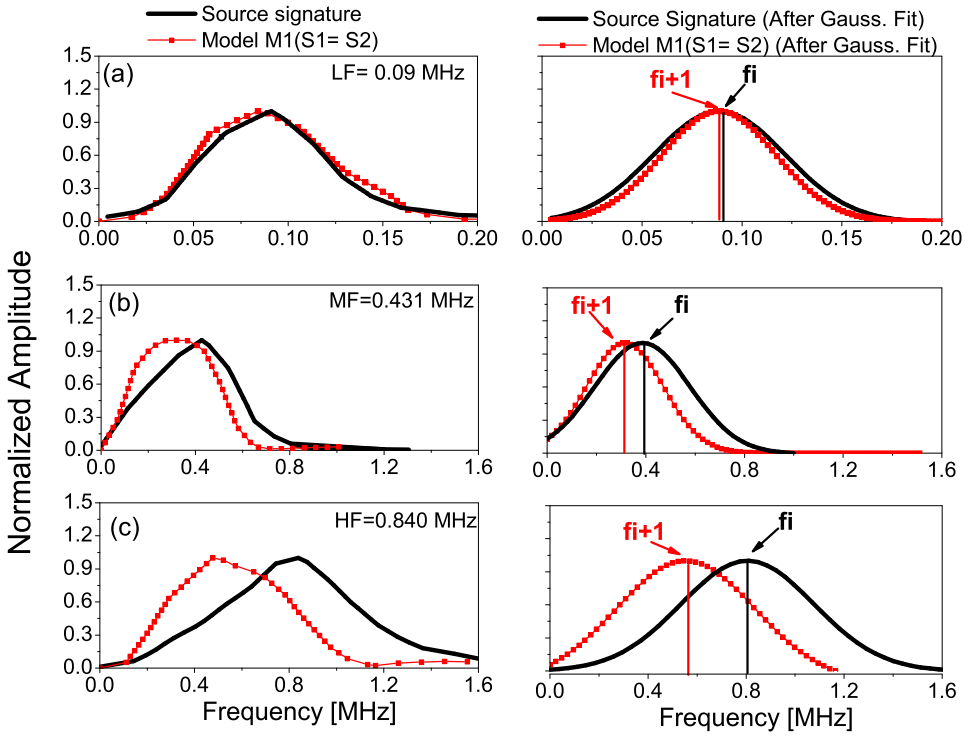

Figure 7: Fourier spectra for model M1 using S-wave sources (a) LW, (b) IF and (c) HF environments.

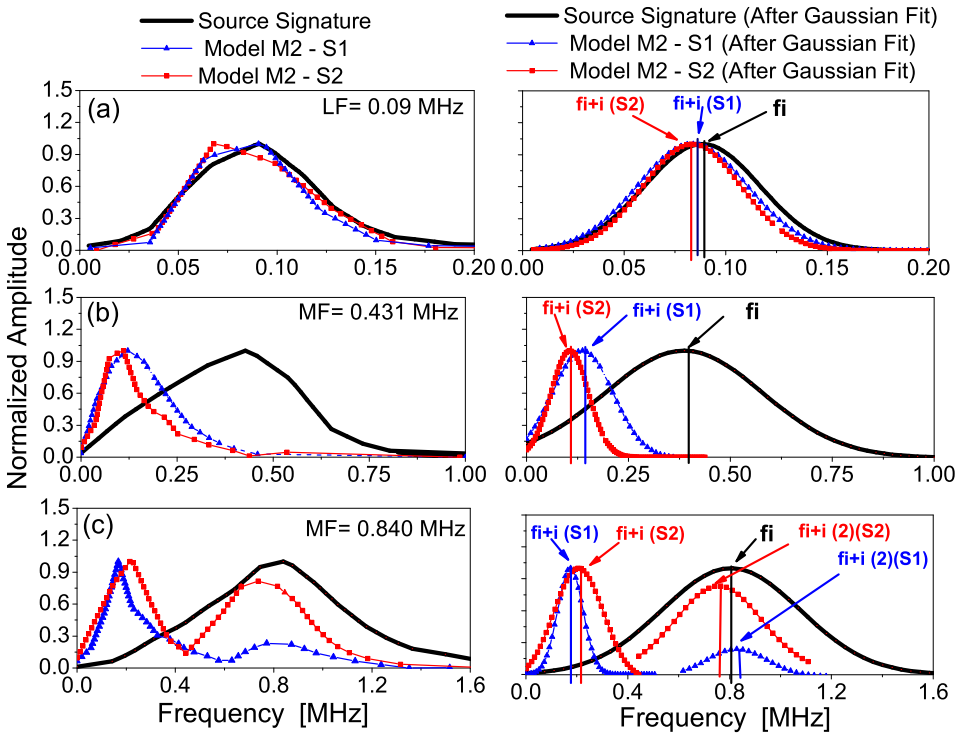

Figure 8: Fourier spectra for model M2 using S-wave sources (a) LW, (b) IF and (c) HF environments.

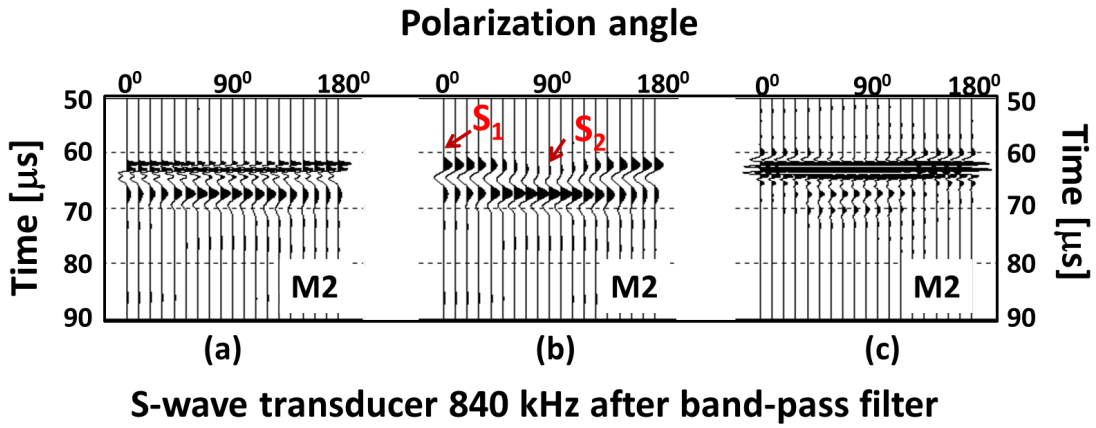

Figure 9: (a) S-wave seismogram for model M2 (b) The same data after application of band-pass filter 10-50-350-400 kHz (S-wave splitting is 1.4 μs). (c) High-frequency section after subtraction of (b) from (a).

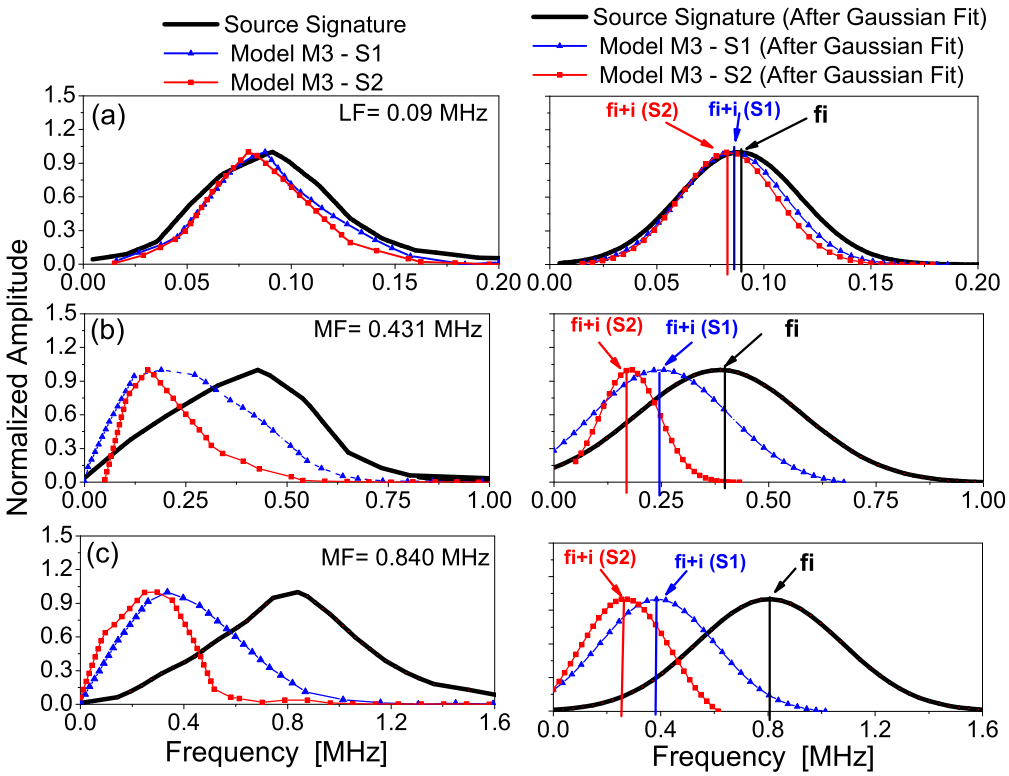

Figure 10: Fourier transform spectra for model M3 using S-wave sources (a) LW, (b) IF and (c) HF environments.

Velocity results

Figure 11 depicts the velocities V_{S1} of the fast shear-wave and V_{S2} of the slow-shear-wave as functions of source transducer frequency. The dispersion effect is more prominent for model M2. It can be noted that in all cracked models the S2 wave is more dispersive.

From these velocity values, we can calculate Thomsen's anisotropy parameter γ from the relationship

$$\gamma = \frac{1}{2}\left(\frac{V_{S1}^2}{V_{S2}^2} - 1\right). \tag{2}$$

Figure 12 shows the anisotropy parameter γ for models M2 and M3. The graph shows that γ decreases with

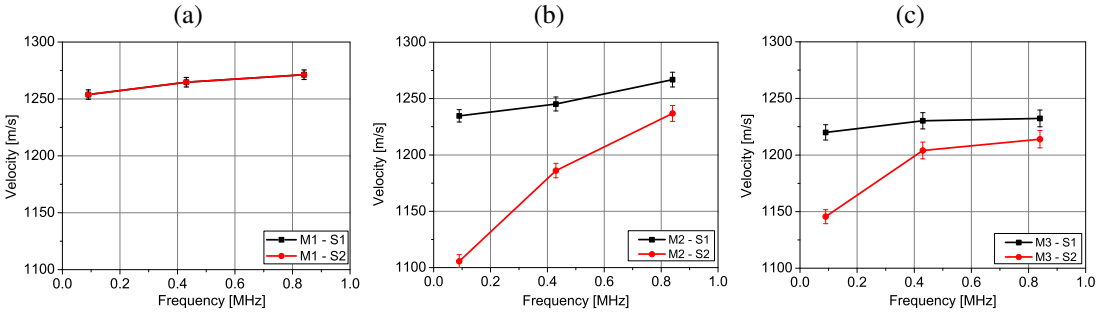

Figure 11: Velocity plots for models M1 (a), M2 (b) and M3 (c) as a function of frequency. The dispersion curves shows the polarization S2 to be more influenced by frequency in model M2.

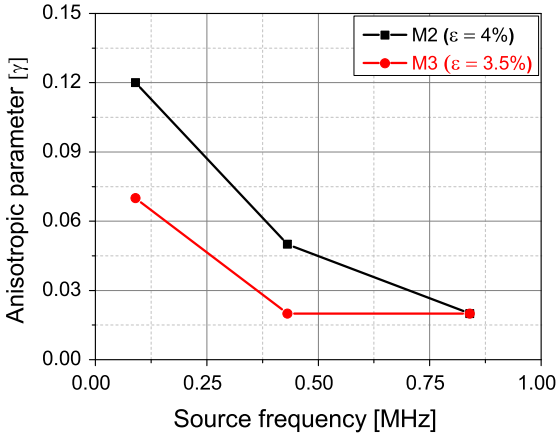

Figure 12: Anisotropy parameter γ calculated from equation (2).

increasing source frequency. For both cracked models, splitting is more pronounced at the lowest frequency (90 kHz) used in this study. As expected from the anisotropic theories for cracked media (Hudson, 1981; Crampin, 1984), the value of $\gamma = 12.2\%$ in model M2, which has a higher crack density than model M3, is higher than $\gamma = 7.2\%$ in model M3.

However, at the highest frequency, the value of $\gamma = 3.0\%$ in model M2 is smaller than the one for M3, $\gamma = 4.2\%$. This evidence shows how the scattering effect can lead to contradictions to the anisotropic theories. From Figure 12, we can infer a relationship between anisotropy and seismic frequency (or wavelength) relative to crack size. At long wavelengths (LF), the effective anisotropy is higher (see 2).

We conclude from these velocity results that the magnitude of shear-wave splitting not only depends on frequency as well as crack size and density alone. It is also influenced directly by scattering attenuation, which in turn depends on frequency and crack size and density.

Model M4. The above observations are confirmed from the results in model M4. Figure 13 shows the velocity of shear-waves (S1 and S2) obtained for model M4. In this model, all cracks have the same aperture (0.091 cm), but three different aspect ratios (0.13, 0.20 and 0.28). The physical informations this model also is contained in Table 1. To separately interpret the S1 and S2 waves in the HF seismograms, we applied again the 10-50-350-400 kHz band-pass filter.

As shown in Figure 13, S-wave splitting does not show a strong dependency on the physical crack parameters. In Figure 13a and b, where long wavelengths are dominant, the anisotropic parameter slightly decreases with reduced crack density and individual crack length. On the other hand, for high frequency (see Figure 13c), a decrease in crack density and crack size leads to a slight increase in magnitude of the anisotropy parameter γ. Thus, we conclude that for high frequencies the crack size is slightly more influential than for low frequencies.

Table 3 summarizes the above results. It shows the velocity values of S1 and S2 waves in models M1, M2, M3, and M4 together with the relevant physical crack parameters diameter, aperture, and density. We see that a simultaneous decrease in diameter, aperture, and density, from model M2 to M3, led to

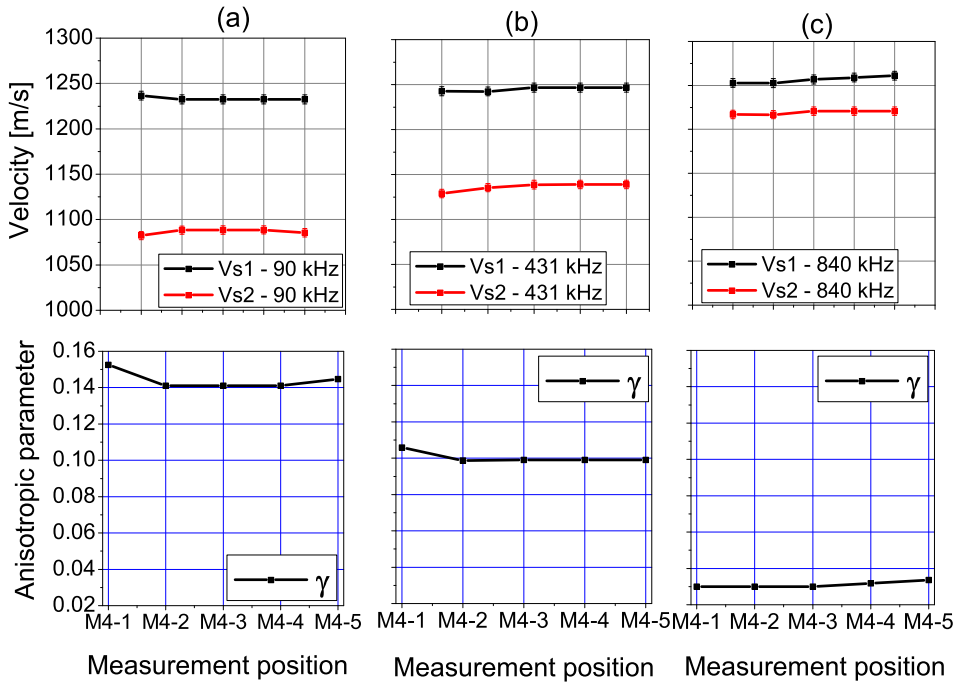

Figure 13: Velocities for five different points in model M4 and the respective anisotropic parameter γ associated with these velocities for S-wave source transducers: (a) LF, (b) IF, and (c) HF ranges.

Source frequency (kHz)				90		431		840	
Model	Crack parameters			Shear-wave velocities					
	Diameter (cm)	Aperture (cm)	Density (%)	$V(S_1)$ (m/s)	$V(S_2)$ (m/s)	$V(S_1)$ (m/s)	$V(S_2)$ (m/s)	$V(S_1)$ (m/s)	$V(S_2)$ (m/s)
M1	-	-	-	1254	1254	1264	1264	1271	1271
M2	0.7	0.091	4.5	1235	1106	1245	1186	1267	1237
M3	0.4	0.051	3.8	1220	1146	1230	1204	1232	1214
M4-1	0.7	0.091	6.0	1237	1082	1243	1129	1253	1217
M4-3	0.44	0.091	5.2	1232	1088	1247	1139	1257	1221
M4-5	0.32	0.091	5.2	1233	1086	1247	1139	1261	1221

Table 3: Velocity values for models M1, M2, M3, and M4 and relations with crack diameter and crack aperture.

decreasing S1 and HF S2 velocities, while only LF and IF S2 velocities increased as expected. On the other hand, from the measuring points M4-1, M4-3, and M4-5, we see that the velocities are practically insensitive to the crack diameter. Slight velocity variations seem to be correlated with the decreasing crack density. Comparing the values for M2 with those for M4-1, we see no sensitivity of LF and IF S1 velocities to crack density, while S2 velocities consistently decrease with increasing density. From the observed dependencies of the shear-wave velocities on the physical crack parameters, we conclude that the crack aperture is the most important parameter for shear-wave splitting, followed by crack density. The crack diameter seems to have the least influence.

Shear-wave attenuation measurement

There are many difficulties that are encountered in the laboratory and field to accurately measure an attenuation value. Effects related to the near-field, spherical divergence, boundaries, reflectors, coupling and scattering are factors that change the amplitude of a seismic trace. To avoid these effects, we used a method that basically depends on the frequency shift observed in the direct-arrival measurements at two different

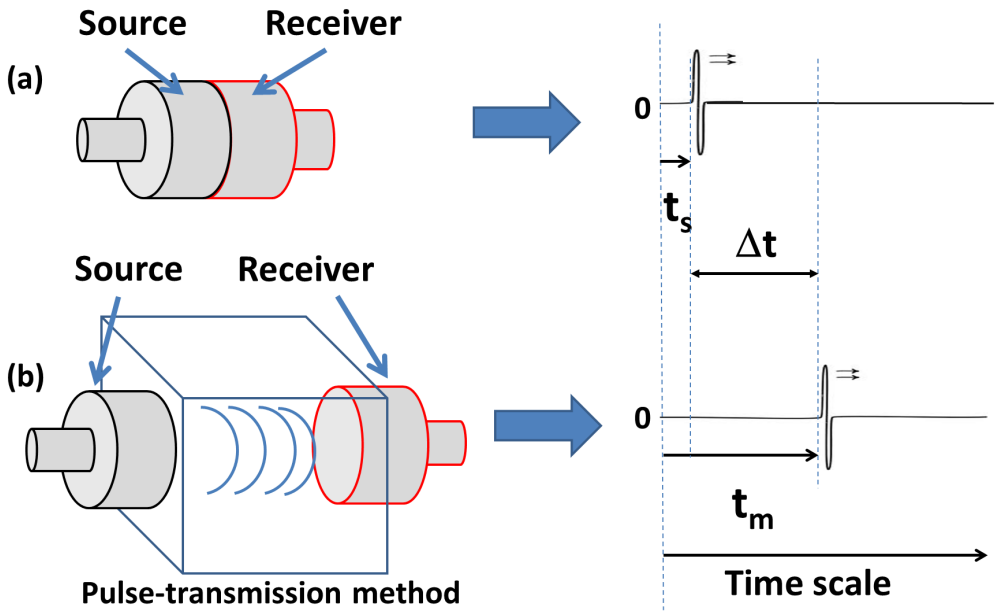

Figure 14: Schematic representation of two recording with different source/receiver spacing. (a) Signature source trace and (b) pulse-transmission trace.

spacings. This method, which does not require any amplitude ratio approach (like, e.g., the spectral ratio), was established by Quan and Harris (1997). The application of this method requires two wave traces registered at two different position.

We applied this method using a source signature trace and the first arrival from the pulse-transmission experiment . The experimental setup is depicted schematically in Figure 14. The frequency shift between the two events determines the Q factor from (Matsushima et al., 2008, 2011)

$$Q = \frac{\sigma_s^2 \pi \Delta t}{\Delta f}\,, \tag{3}$$

where Δt is the traveltime difference between two different recordings as depicted in Figure 14, $\Delta f = (f_s - f_m)$ is the difference in centroid frequency between the source and the model-trace pulse (as depicted in Figure 14) after Gaussian non-linear fit and σ_s^2 is the variance of the source frequency. Table 4 shows the centroid frequencies and respective variances of sources in the different frequency ranges, as well as the centroid frequencies of models M1, M2, M3 for polarizations S1 and S2.

Source frequency (kHz)		90		431		840	
Centroid frequency f_s (kHz)		88.4		386		805	
Variance σ_s (kHz)		38.5		193		271	
Model-trace	Model	S1	S2	S1	S2	S1	S2
centroid	M1	87.5	87.5	317	317	552	552
frequency f_m	M2	84.3	83.2	137	106	172	206.5
(kHz)	M3	85.4	83.5	249	176	386	266

Table 4: Source centroid frequencies f_s and respective variances σ_s, as well as model-trace centroid frequencies f_m of models M1, M2, M3 for polarizations S1 and S2.

Using the values from table 4 and the first arrival traveltimes of the S1 and S2 waves in the seismic profiles shown in Figures 4, 5, and 6, we calculate the total attenuation Q^{-1} using equation (3). The result is depicted in Figure 15. Errors are estimated from the neighboring traces. We see that in all models the attenuation increases with increasing frequency, and for low to intermediate frequencies, the increase in the

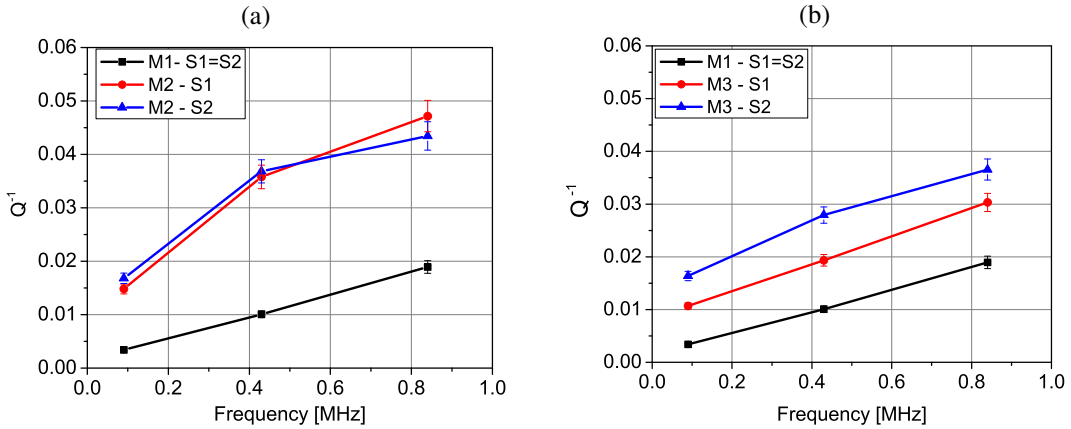

Figure 15: Total attenuation Q^{-1}. (a) Comparison of attenuation in models M1 and M2. (b) Comparison of attenuation in models M1 and M3.

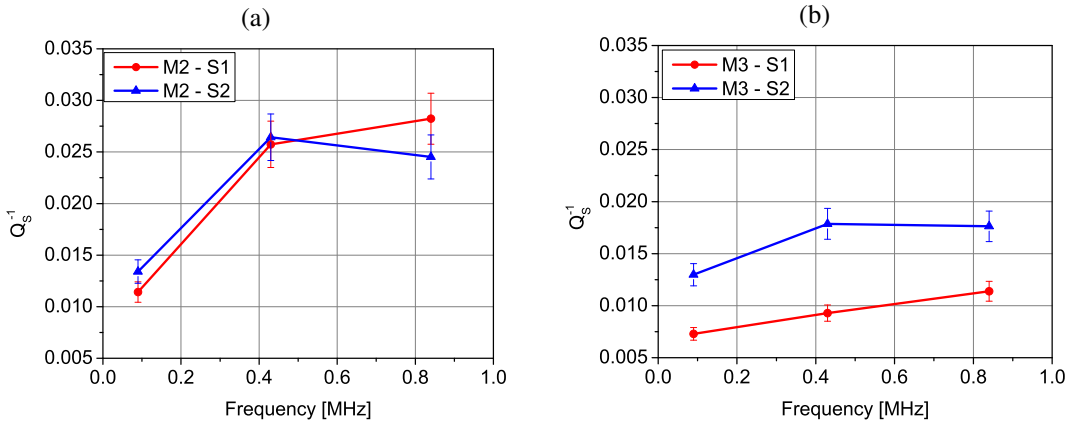

Figure 16: Scattering attenuation Q_s^{-1} for models M2 (a) and M3 (b) for the shear-wave polarizations S1 and S2.

cracked models M2 and M3 is stronger than in the isotropic model M1. In models M3, the behavior of the two polarizations is not significantly different, but differs distinctly from that in model M1. In model M2, the S2 wave is significantly stronger attenuated than the S1 wave.

Next, we calculated the scattering attenuation using the approach of Brown and Seifert (1997) and Tselentis (1998). For this purpose, we subtract the intrinsic attenuation Q_{in}^{-1} in model M1 (model without inclusions) from the total attenuation Q^{-1} for models M2 and M3, i.e.,

$$Q_s^{-1} = Q^{-1} - Q_{in}^{-1} \tag{4}$$

Figure 16 shows that the so-obtained scattering attenuation Q_s^{-1} for both (fast and slow) polarizations increases with increasing source frequency from LF to IF in both models M2 and M3. While the scattering attenuation continues to increase for S1 from IF to HF, it remains approximately constant for S2 in model M3 or even slightly decreases in model M2. This latter behaviour is consistent with our previous interpretation that for very high frequencies, there are waves that propagate in the space between the cracks in the isotropic background medium.

All our above observations indicate that the S2 wave is more strongly influenced by cracks in the medium when the propagation is closer to the effective-medium condition, i.e. for low and intermediate frequencies.

CONCLUSIONS

This experimental study has investigated the influence of frequency in anisotropic media containing aligned penny-shaped cracks. The results show that S-wave splitting directly depends on the source frequency as

well as crack size and density. In the low-frequency range, splitting was more conspicuous in all cracked models than at higher frequencies. In the high-frequency range, the magnitude of S-wave splitting decreases drastically. Low-pass filtering of high-frequency data turned out to be helpful to make a small shear-wave splitting visible. This splitting was higher for larger cracks with smaller density.

We observed the dispersive effect of cracked media to be higher for the S2 than the S1 polarization. It predominates when the crack length is smaller or of the same order as the wavelengths used in the investigation. Moreover, the lower the source frequency was, the more pronounced were the observed dispersive effects.

Contrary to the typical behaviour of shear-wave splitting, the S1 wave seems to be more influenced by scattering than S2 when the crack size is larger than the wavelength. If this statement can be confirmed by future experiments, the crack aperture may be less relevant than the individual crack size in the HF range. An additional experminent with constant crack density and aperture but varying crack size in the high-frequency range also showed an increasing anisotropy parameter with decreasing crack size.

From our experiments, we can establish an order of importance of different physical crack parameters for shear-wave propagation. The results show that the crack aperture is the most relevant parameter, followed by crack density. Crack size seems to have the least influence on shear-wave velocities. Even in the low-frequency case, where the S-wave propagation behaves like in an effective medium, the anisotropic parameter γ does not strongly depend on the crack size.

ACKNOWLEDGEMENTS

This work was made possible by the Allied Geophysics Laboratories financial support. The authors are grateful to Dr. Leon Thomsen and Dr. Evgeny Chesnokov for them expertise advice. The first author wishes to thank CAPES and CNPq from Brazil for his scholarship (contract # 201461/2009-9). Also, we are grateful to Petrobras and the sponsors of the *Wave Inversion Technology (WIT) Consortium*.

REFERENCES

Assad, J. M., Mcdonald, J. A., Tatham, R. H., and Kusky, T. M. (1996). Elastic wave propagation in a medium containing oriented inclusions with a changing aspect ratio: A physical model study. *Geophysical Journal International*, 125(1):163–172.

Assad, J. M., Tatham, R. H., and Mcdonald, J. A. (1992). A physical model study of microcrack-induced anisotropy. *Geophysics*, 57:1562.

Brown, R. L. and Seifert, D. (1997). Velocity dispersion: A tool for characterizing reservoir rocks. *Geophysics*, 62:477.

Crampin, S. (1981). A review of wave motion in anisotropic and cracked elastic-media. *Wave Motion*, 3(4):343–391.

Crampin, S. (1984). Effective anisotropic elastic constants for wave propagation through cracked solids. *Geophysical Journal of the Royal Astronomical Society*, 76(1):135–145.

Gibson, R. L., Theophanis, S., and ToksoÌĹz, M. N. (2000). Physical and numerical modeling of tuning and diffraction in azimuthally anisotropic media. *Geophysics*, 65:1613.

Gorich, U. and Muller, G. (1987). Apparent and intrinsic Q: the one–dimensional case. *J. Geophys.*, 61:46–54.

Hudson, J. A. (1981). Wave speeds and attenuation of elastic waves in material containing cracks. *Geophysical Journal of the Royal Astronomical Society*, 64(1):133–150.

Hudson, J. A., Pointer, T., and Liu, E. (2001). Effectiv-medium theories for fluid-saturated materials with aligned cracks. *Geophysical Prospecting*, 49(5):509–522.

Mal, A. K. (1970). Interaction of elastic waves with a penny-shaped crack. *International Journal of Engineering Science*, 8(5):381–388.

Marion, D., Mukerji, T., and Mavko, G. (1994). Scale effects on velocity dispersion: From ray to effective medium theories in stratified media. *Geophysics*, 59:1613.

Matsushima, J., Suzuki, M., Kato, Y., Nibe, T., and Rokugawa, S. (2008). Laboratory experiments on compressional ultrasonic wave attenuation in partially frozen brines. *Geophysics*, 73:N9.

Matsushima, J., Suzuki, M., Kato, Y., and Rokugawa, S. (2011). Estimation of ultrasonic scattering attenuation in partially frozen brines using magnetic resonance images. *Geophysics*, 76:T13.

Melia, P. J. and Carison, R. L. (1984). An experimental test of p-wave anisotropy in stratified media. *Geophysics*, 49:374.

Peacock, S., McCann, C., Sothcott, J., and Astin, T. R. (1994). Seismic velocities in fractured rocks: an experimental verification of hudson's theory. *Geophysical Prospecting*, 42(1):27–80.

Quan, Y. and Harris, J. M. (1997). Seismic attenuation tomography using the frequency shift method. *Geophysics*, 62:895.

Rathore, J. S., Fjaer, E., Holt, R. M., and Renlie, L. (1995). P- and S- wave anisotropy of a synthetic sandstone with controlled crack geometry. *Geophysical Prospecting*, 43(6):711–728.

Rio, P., Murkeji, T., Mavko, G., and Marion, D. (1996). Velocity dispersion and upscaling in a laboratory-simulated VSP. *Geophysics*, 61:584.

Thomsen, L. (1986). Weak elastic anisotropy. *Geophysics*, 51:1954.

Thomsen, L. (1995). Elastic anisotropy due to aligned cracks in porous rock1. *Geophysical Prospecting*, 43(6):805–829.

Tillotson, P., Chapman, M., Best, A. I., Sothcott, J., McCann, C., Shangxu, W., and Li, X. (2011). Observations of fluid - dependent shear - wave splitting in synthetic porous rocks with aligned penny - shaped fractures. *Geophysical Prospecting*, 59(1):111–119.

Tselentis, G. (1998). Intrinsic and scattering seismic attenuation in w. greece. *Pure and Applied Geophysics*, 153:703–712.

Wei, J. (2004). A physical model study of different crack densities. *Journal of Geophysics and Engineering*, 1:70–76.

Wei, J., Di, B., and Li, X. (2007). Effects of fracture scale length and aperture on seismic waves: An experimental study. pages 169–173.

Willis, J. R. (1964). Anisotropic elastic inclusion problem. *The Quarterly Journal of Mechanics and Applied Mathematics*, 17(2):157 –174.

Yang, L. and Turner, J. A. (2003). Elastic wave propagation and scattering in solids with uniaxially aligned cracks. *The Journal of the Acoustical Society of America*, 114:591.

Yang, L. and Turner, J. A. (2005). Wave attenuations in solids with perfectly aligned cracks. *Acoustics Research Letters Online*, 6:99.